J Mater Sci (2012) 47:227–233
DOI 10.1007/s10853-011-5789-9

$LaCrO_3$–VO_x–YSZ anode material for solid oxide fuel cells operating on H_2S-containing syngas

Cheng Peng · Binwei Wang · Adrien Vincent

Received: 7 April 2011 / Accepted: 12 July 2011 / Published online: 21 July 2011

Abstract The perovskite type lanthanum chromite $LaCrO_3$ has been synthesized by nitrate-citrate combustion method. Phase transformations have been studied by using simultaneous differential scanning calorimetry and thermogravimetric analysis. The bulk structure of $LaCrO_3$ as well as the catalyst have been examined by X-ray diffraction (XRD). The cell was made using $LaCrO_3$–VO_x–YSZ anode. Impedance measurements showed that the polarization resistance was much smaller when the fuel changed from pure H_2 to 5000 ppm H_2S balance H_2. The performance for 5000 ppm H_2S balance H_2 was much better than with pure H_2 as a result of a lower polarization resistance. At 900 °C the maximum power density was 463 mW cm^{-2} when using H_2S-containing H_2 as fuel. The presence of H_2S in the syngas significantly decreased the polarization resistance and improved the fuel cell performance. At 900 °C the achieved power density was 214 mW cm^{-2} for H_2S (5000 ppm)-containing syngas (40% CO + 60% H_2).

Introduction

Solid oxide fuel cells (SOFCs) is a very promising candidate for future energy conversion device because it can directly convert the chemical energy of the fuel into electrical energy in a very high efficient and environmentally benign way [1, 2]. A major issue considering a future commercialization of SOFCs is the requirement of pure hydrogen or hydrogen-rich fuel. Recently, many researches based on SOFCs development were focused on using basic hydrocarbon fuels instead of pure hydrogen. However, the H_2S contained in the commercially available hydrocarbon fuels seriously damage the commonly used anode material [3–6]. Therefore, the development of an alternative H_2S-tolerant anode material is required when directly using hydrocarbon fuels.

Owing to its low cost, syngas is a typical alternative fuel mainly produced by gas reforming of hydrocarbons. The interest for using syngas as the fuel for SOFCs recently rose significantly to make it one of the top research interests [4, 7–9]. But until now H_2S-containing syngas is seldom studied as a fuel for SOFCs.

The ideal anode material for syngas SOFCs must be a good electronic and ionic conductor with a good chemical and thermal stability. At the same time it must be catalytically active for the electrochemical oxidation of H_2S, H_2, and CO. For a single material it is very hard to meet all these requirements. So we chose to focus on a composite material. Vanadium oxide-based material has exhibited a large potential for the selective oxidation and oxidative dehydrogenation of hydrocarbons [10–13]. It has also been used for oxidation of H_2S and SO_2 [14, 15]. At the same time the reducing atmosphere in the anode compartment will keep the vanadium oxide with low valence level, which has a much higher melting point than vanadium pentoxide (690 °C). The lanthanum chromite $LaCrO_3$ has presented a high melting point, high electrical conductivity and high catalytic oxidation activity, as well as a high thermal and chemical stability [16–19]. Such properties make them very attractive as an anode component for the wanted applications. In order to provide a good ionic

C. Peng (✉) · B. Wang
College of Materials Science and Engineering, Huaqiao University, 361021 Xiamen, People's Republic of China
e-mail: chengpeng@hqu.edu.cn

A. Vincent
Department of Chemical and Materials Engineering, University of Alberta, Edmonton T6G 2G6, Canada

conductivity, YSZ was also included in the composite anode. Within this context, we have chosen $LaCrO_3$–VO_x–YSZ composite material as an anode catalyst for syngas SOFCs.

In this study, H_2S (5000 ppm)-containing syngas (40% CO + 60% H_2) was used as the fuel over $LaCrO_3$–VO_x–YSZ composite anode. The current–voltage measurements and the impedance tests were performed. The $LaCrO_3$–VO_x–YSZ anode was shown to be a good sulfur tolerant.

Experimental

Catalyst preparation

The $LaCrO_3$ was synthesized by a nitrate-citrate combustion process described elsewhere [20]. The starting materials were $La(NO_3)_2{\cdot}6H_2O$ (Alfa Aesar, 99.9%), $Cr(NO_3)_3$ (Acros Organics, 99%), and citric acid (Acros Organics, 99%). Citric acid was used both as an organic fuel and as a complexant. Indeed, it forms stable water-soluble complexes with La and Cr ions. Nitrate was used as an oxidant. The aqueous solution was adjusted to pH 7 by adding ammonium hydroxide. The solution was dried on a hotplate at 70–80 °C, whereupon it became a translucent gel. The gel was heated further until it turned into a black viscous mass, which then combusted vigorously to produce a very fine powder.

V_2O_5 (Aldrich, 99.9%) was reduced in pure H_2 gas at 500 °C for 8 h to obtain VO_x as a black powder with a Karelianite (V_2O_3) like structure. From XRD patterns, the main peaks for VO_x match the peaks for Karelianite, we use the formula VO_x instead of V_2O_3, as there was also several additional small peaks in the XRD of VO_x, and XPS analysis also shows the presence of more than one V species and different binding energies between O1s and V2p electrons for synthesized VO_x and pure V_2O_3 (Alfa Aesar, 99.9%).

The VO_x, $LaCrO_3$, and 8 mol% YSZ nanopowder (Inframat Advanced Materials) were intimately mixed in a 2:2:1 weight ratio in isopropanol (Fisher, 99.5%) in an ultrasonic bath for 1 h. The dry composite anode catalyst $LaCrO_3$–VO_x–YSZ remained after natural evaporation of isopropanol at room temperature.

Cell preparation

Dense commercial 8 mol% YSZ pellet (25 mm in diameter and 0.3 mm in thickness, NexTech Materials. Ltd) was used as the electrolyte. Porous platinum was used as cathode catalyst, prepared by screen printing platinum paste (Heraeus CL11-5100) on one side of the YSZ pellet. After drying in air for 3 h, it was then heated at 850 °C for 30 min to remove the organic medium and form the porous cathode. The $LaCrO_3$–VO_x–YSZ anode material was mixed with α-terpineol (Heraeus-372) to form a viscous ink that was screen printed on to the other side of the YSZ pellet. The electrode was then fired in situ at 900 °C before any test from the cell. The apparent anode surface area was 1 cm^2 and the anode thickness was approximately 0.1 mm.

Current collectors comprising gold meshes welded to a gold wire were placed in intimate contact with the surface of each electrode. The membrane assembly so formed was secured between two coaxial alumina tubes to form the anode and cathode compartments. Ceramic sealant (Ceramabond 503, Aremco) was applied on both sides of the electrolyte to seal the gas compartments. The cell was heated in a tubular furnace (Thermolyne F79300). Air and nitrogen initially flowed through the cathode and anode chambers, respectively. Once the operating temperature was reached, nitrogen was switched to fuel gas.

Electrochemical measurement

A Solartron Electrochemical interface (S1 1287) was used in all of the tests to monitor the open circuit voltage (OCV) between anode and cathode, and to measure current–potential performance and electrochemical impedance. Potentiodynamic mode was used to perform current–potential measurements. The scanning rate was kept at 5 mV/s. Impedance data were obtained over the frequency range 1 MHz to 0.1 Hz. The cell was stabilized until the OCV achieved a stable value after each change in operating conditions before any further measurements.

Fuel cell performance and impedance measurements were determined in the H_2S (5000 ppm)-containing syngas (40% CO + 60% H_2). We chose 5000 ppmv H_2S because diesel fuel in the United States may contain up to 5000 ppm sulfur and this value is also a typical sulfur concentration in syngas derived from coal [21].

Materials characterization

Crystal phase identification of synthesized materials was performed using a Siemens D5000 X-ray diffractometer with Ni filtered Co K_α radiation. Morphology and microstructure of the samples as well as elemental analyses were determined using SEM/EDX techniques with a Hitachi S-2700 scanning electron microscope (SEM) and PGT Imix system with a PRISM IG. The thermal decomposition of the dried gel precursor was investigated by differential scanning calorimetry (DSC) and thermogravimetric analysis (TGA) between 25 and 1000 °C with a TA SDT-Q600 instrument at a heating rate of 10 °C min^{-1} in air (flow rate: 100 mL min^{-1}).

Results and discussion

Thermogravimetric analysis and phase structure of $LaCrO_3$

Phase transformations were studied by using simultaneous differential scanning calorimetry and thermogravimetric analysis. The TGA/DSC curve of the precursor gel is presented in Fig. 1. As can be seen in the DSC plot, we observe a strong and a weak endothermic peaks at about 200 and 230 °C, respectively. Then around 273 °C a weak exothermic peak appeared followed by a strong one near 447 °C. The weight loss below 250 °C is assigned to the loss of residual water molecules in the sample. The second apparent weight loss occurred between 250 and 450 °C in coincidence with the observation of a relatively large exothermic peak centered at 450 °C. After the initial loss of water from the precursor, the decomposition of the citrate by decarboxylation is expected. At the same time the burning of the residual organic matter in the sample and the gradual crystallizing process of $LaCrO_4$ might be also happened during this exothermic process.

The TG result indicates the weight loss is nearly completed around 460 °C. The temperature for completion of weight loss is considerably lower than that of sol–gel derived lanthanum chromite perovskite (around 800 °C) [22]. This indicates that the phase pure powder can be prepared at a lower temperature.

The TGA/DSC data in Fig. 1 also shows a structure transformation occurring at around 730 °C. Coupled to an endothermic peak in the DSC curve, the TGA curve shows a weight loss which correspond to the partial $LaCrO_4$ to $LaCrO_3$ transformation, which is in agreement with XRD results discussed below. No other interactions or weight changes occurred as the temperature increased to 1000 °C.

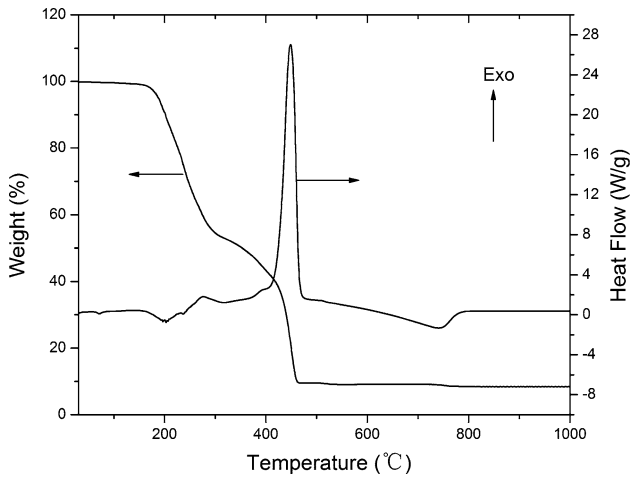

Fig. 1 TGA/DSC curve of the dried precursor gel

The $LaCrO_3$ phase evolution during the gel-combustion process as a function of heat-treatment temperature was examined by XRD (Fig. 2). For gel combustion sample it can be seen that $LaCrO_4$ phase has formed just after combustion process. At the same time the peaks marked with an empty circle indexed as $LaCrO_4$ standard (JCPDS card no. 49-1710) are observable in the diffraction pattern. After heated at 800 °C for 1 h in air the XRD data show no evidence of impurity and only one crystalline phase corresponded to a monoclinic perovskite structure appeared, as compared to $LaCrO_3$ standard (JCPDS card no. 24-1016) and commercial $LaCrO_3$ (Alfa Aesar, 99.5%). Low temperature for the formation of the perovskite phase indicates an intimate level mixing among starting reactants, which leads to a short diffusion distance and a homogenous product as well.

The SEM micrograph of $LaCrO_3$ powder made by nitrate-citrate combustion synthesis after heat treatment at 800 °C for 1 h in air is presented in Fig. 3. The grain size of the powder is in the range of 100–150 nm with a very narrow distribution. A large amount of gases produced during the combustion process and the rapid combustion reaction rate both can limit the growth of crystallite, which will keep the nano-scale size of the initial product. At the same time it can also be seen from this figure that the particles were connected to each other in agglomerates of different shapes and sizes.

Phase structure of the anode catalyst and microstructure of the cell assembly

Figure 4 shows the XRD pattern of the as-prepared anode catalyst. The peaks marked with an asterisk correspond to

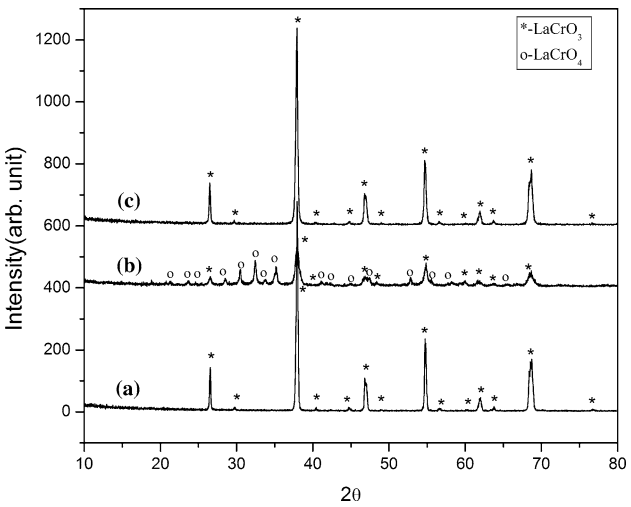

Fig. 2 Thermal evolution of the powder X-ray diffraction spectrum of $LaCrO_3$: **a** commercial $LaCrO_3$ powder, **b** gel combustion product, **c** sample after heated at 800 °C for 1 h in air

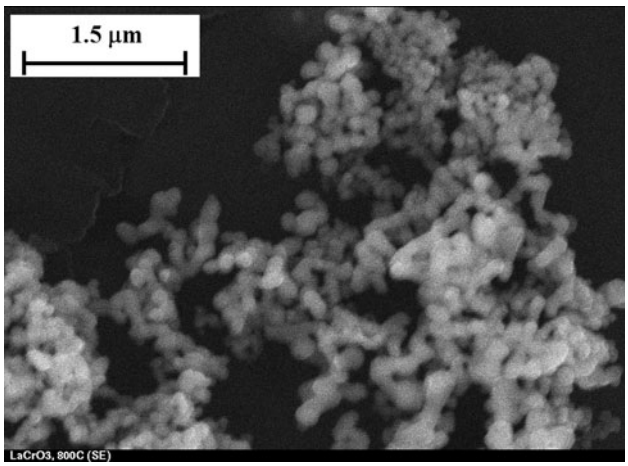

Fig. 3 SEM micrograph of $LaCrO_3$ powder made by citric-nitrate combustion synthesis after heat treatment at 800 °C for 1 h in air

the lanthanum chromite, as compared with the $LaCrO_3$ standard (JCPDS card no. 24-1016). The peaks marked with a number sign correspond to the vanadium oxide, as compared with the Karelianite (JCPDS card no. 34-0187). The peaks marked with an open circle correspond to the YSZ, as compared with the YSZ standard (JCPDS card no. 48-0224).

Figure 5a gives an overall cross-sectional view of a fractured cell. The thickness of the anode catalyst layer was approximately 100 μm. The cathode catalyst layer was very thin compared to the thickness of the anode catalyst layer. From Fig. 5b, c, the anode catalyst had uniform porous microstructure, which will provide a better surface area and an easy mass transfer within the anode catalyst layer. At the same time it can be seen that there was a good contact and distribution for the anode component, which was also confirmed by the EDX. Fine needles are nano-scale YSZ grains. Finally, a porous microstructure was also observed for the cathode catalyst (Fig. 5d).

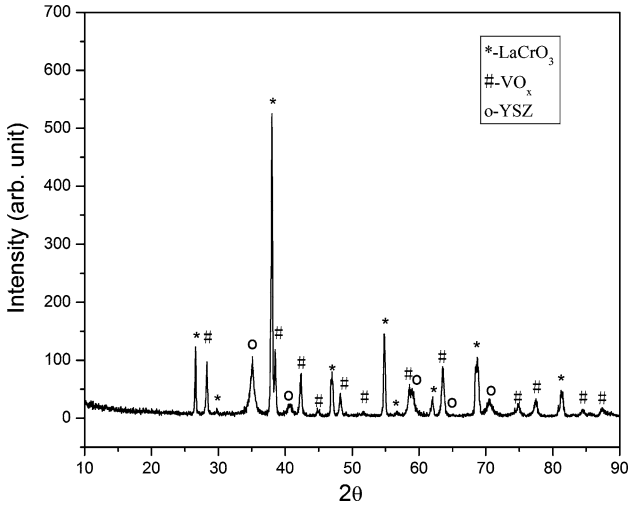

Fig. 4 XRD patterns of the as-prepared anode catalyst

The effect of H_2S on the performance of single cell fed with H_2

The single cell performance using $LaCrO_3$–VO_x–YSZ as anode and platinum as cathode in pure H_2 and 5000 ppm H_2S balance H_2 were determined and compared. Figure 6 compares the impedance spectra of a single cell at 800 °C in pure H_2 and 5000 ppm H_2S balance H_2. The ohmic resistance was almost the same for these two different fuels. However, the polarization resistance was much smaller when the fuel changed to 5000 ppm H_2S balance H_2. This phenomenon was very consistent over several fuel cycles. Figure 7 shows the I–V curves at 800 °C for cells using the $LaCrO_3$–VO_x–YSZ exposed to pure H_2 and 5000 ppm H_2S balance H_2. The performance for 5000 ppm H_2S balance H_2 was much better than for pure H_2 as a result of much less polarization resistance. At 800 °C the highest power density achieved was 174 mW cm^{-2} when using H_2S-containing H_2 as fuel, compared to the 84 mW cm^{-2} for pure H_2. Similar observations have been reported for MoS_2 catalyst [9]. Higher performance with only 0.5% of H_2S in H_2 might be due to the different adsorption ability on the surface of the anode catalyst for H_2 and H_2S. H_2S might have the priority to adsorb on the catalyst surface and to form sulfur-containing species, which will improve the rate of adsorption and dissociation of H_2 on the catalyst surface.

Figure 8 shows the impedance spectra for $LaCrO_3$–VO_x–YSZ in 5000 ppm H_2S-containing H_2 at different operating temperatures. With increasing the operating temperature the ohmic resistance decreased mainly because of a better electrolyte (YSZ) conductivity. The ohmic resistance was 3.3 Ω at 800 °C, 1.1 Ω at 850 °C, and 0.9 Ω at 900 °C. At the same time the polarization resistance decreased significantly with the temperature rise. Figure 9 shows the IV–IP curves for 5000 ppm H_2S-containing H_2 at different operating temperatures. With increasing temperature the performance improved greatly as a result of decreased polarization and ohmic resistance. The maximum power density was about 463 mW cm^{-2} at 900 °C.

The effect of H_2S on the performance of single cell fed with syngas

Figures 10 and 11 show the comparison of impedance spectra and IV–IP performances for $LaCrO_3$–VO_x–YSZ in 5000 ppm H_2S-containing syngas and pure syngas at 900 °C. From these figures the presence of H_2S in the syngas significantly decreased the polarization resistance and improved the fuel cell performance. The impedance

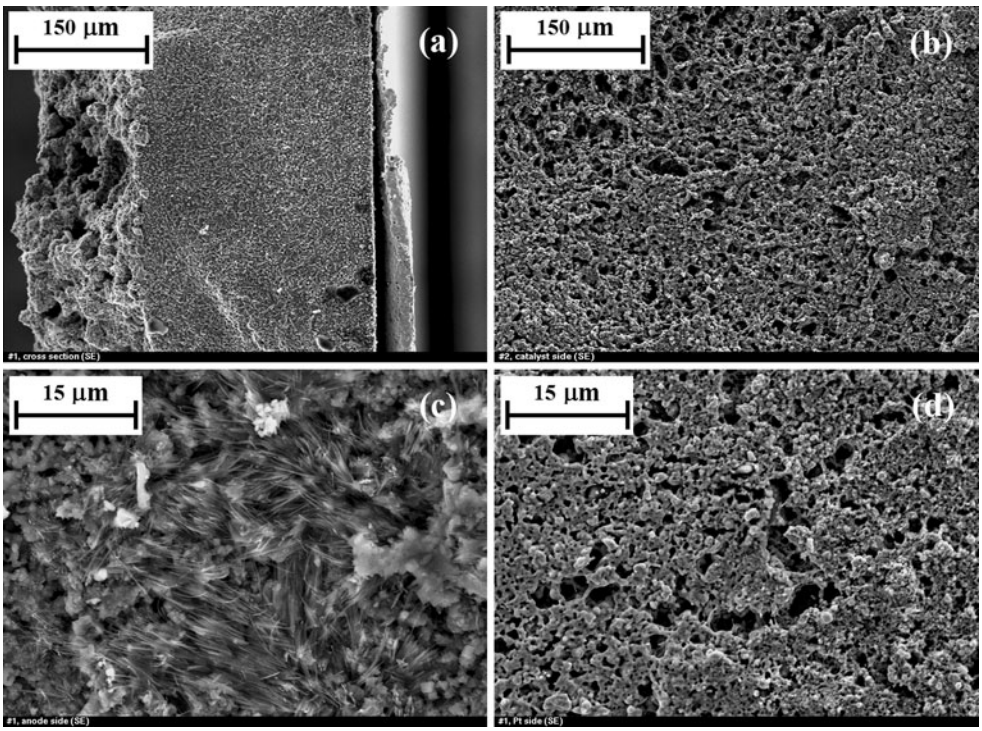

Fig. 5 SEM images of the assembly cross-sectional view (**a**), *top view* for the anode catalyst (**b**, **c**), and cathode catalyst (**d**)

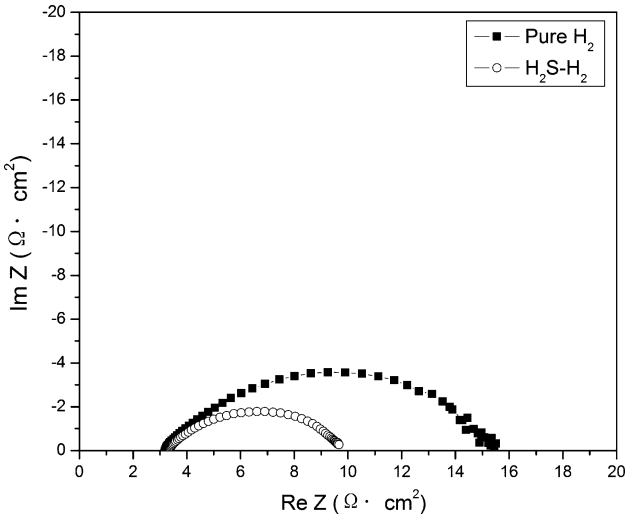

Fig. 6 Impedance spectra for $LaCrO_3$–VO_x–YSZ in pure H_2 and 5000 ppm H_2S-containing H_2 at 800 °C

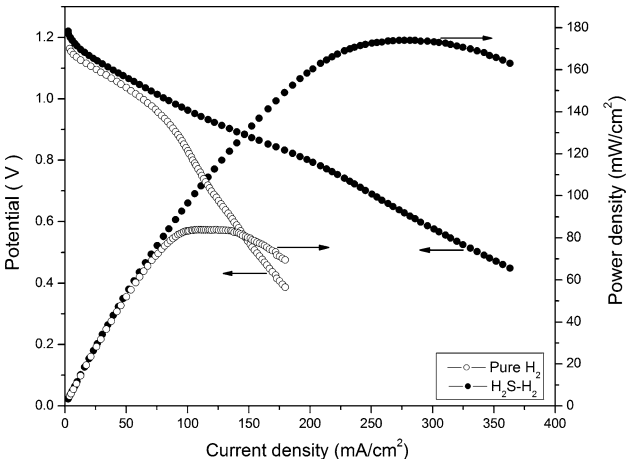

Fig. 7 IV–IP performances at 800 °C for pure H_2 and 5000 ppm H_2S-containing H_2

spectra have also shown that the overall polarization was smaller and the radius shortened when H_2S was injected in the feeding gas. At 900 °C the power density achieved was 214 mW cm^{-2} when using 5000 ppm H_2S-containing syngas compared to the 85 mW cm^{-2} for pure syngas. Until now the exact enhancement mechanism for H_2S is not clear. Further investigation is now being done in our group.

Compared to the performance at 900 °C for 5000 ppm H_2S-containing H_2 (463 mW cm^{-2}), the cell performances for 5000 ppm H_2S-containing syngas are significantly lower. It seems that the presence of CO in the 5000 ppm H_2S-containing H_2 fuel has a negative effect for the cell performance. It can most likely be related to the carbon deposition since CO can form deposition carbon via the disproportionation reaction [23], which will poison the catalyst surface and decrease the cell performance. At the same time this result is in contradiction with Botte's

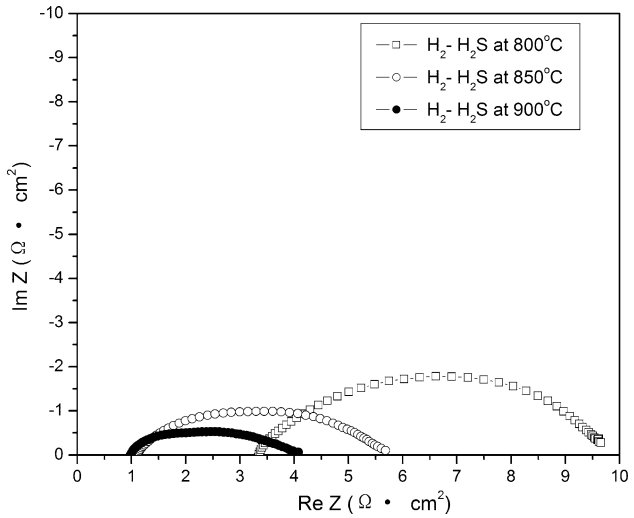

Fig. 8 Impedance spectra for $LaCrO_3$–VO_x–YSZ in 5000 ppm H_2S-containing H_2 at different operating temperatures

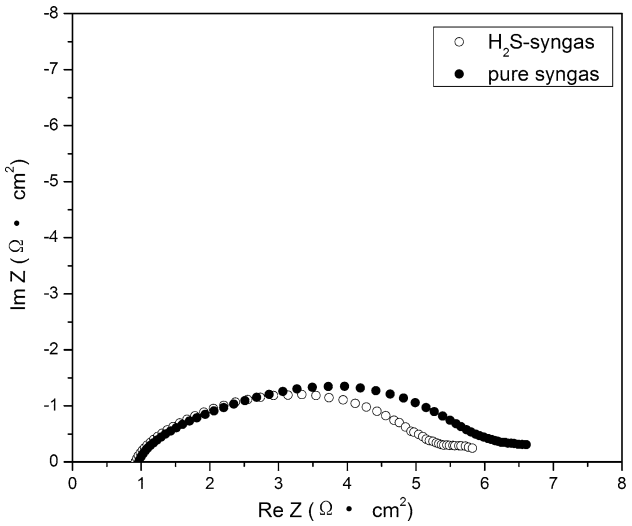

Fig. 10 Impedance spectra for $LaCrO_3$–VO_x–YSZ in pure syngas and 5000 ppm H_2S-containing syngas at 900 °C

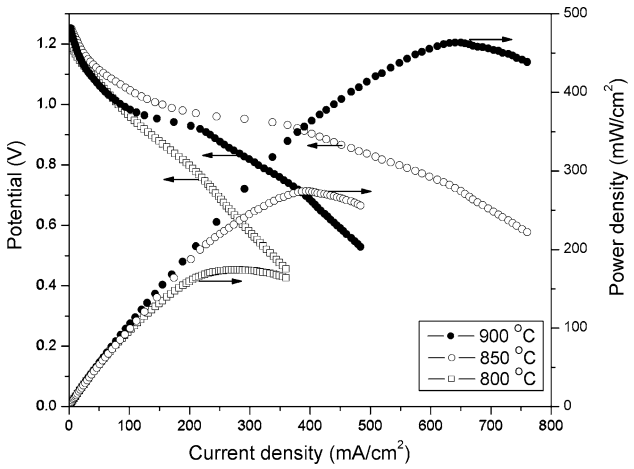

Fig. 9 IV–IP performances for $LaCrO_3$–VO_x–YSZ in 5000 ppm H_2S-containing H_2 at different operating temperatures

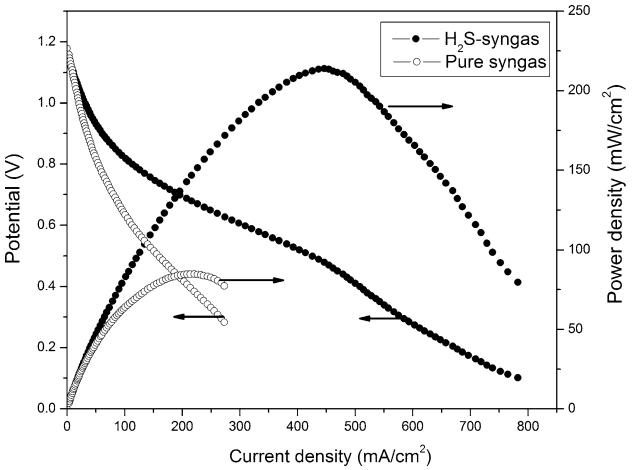

Fig. 11 IV–IP performances at 900 °C for pure syngas and 5000 ppm H_2S-containing syngas

observation, who has found a beneficial synergistic effect among CO, H_2, and H_2S [24].

Conclusions

The perovskite type lanthanum chromite $LaCrO_3$ has been synthesized by nitrate-citrate combustion method. After heated at 800 °C for 1 h in air the XRD data has shown no evidence of impurity and only one pure crystalline phase identified as a monoclinic perovskite structure. The grain size of the powder is in the range of 100–150 nm with a very narrow size distribution.

Impedance measurement showed that the polarization resistance was smaller when the fuel changed from pure H_2 to 5000 ppm H_2S balance H_2. The performances for 5000 ppm H_2S balance H_2 were much better than pure H_2 as a result of a lower polarization resistance. With increasing temperature the cell performance in 5000 ppm H_2S balance H_2 improved greatly as a result of decreased polarization and ohmic resistance. The maximum power density was about 463 mW cm^{-2} at 900 °C.

The presence of H_2S in syngas significantly decreased the polarization resistance and improved the fuel cell performance. At 900 °C the achieved power density was 214 mW cm^{-2} using 5000 ppm H_2S-containing syngas compared to the 85 mW cm^{-2} for pure syngas. The presence of CO in the 5000 ppm H_2S-containing H_2 fuel has a negative effect on the cell performance.

Acknowledgements This study was supported by Scientific Research Fund of Huaqiao University (No. 10Y0195*) and The

Project Sponsored by the Scientific Research Foundation for the Returned Overseas Chinese Scholars, State Education Ministry.

References

1. Atkinson A, Barnett S, Gorte RJ, Irvine JTS, McEvoy AJ, Mogensen M, Singhal SC, Vohs J (2004) Nat Mater 3:17
2. Sasaki K, Susuki K, Iyoshi A, Uchimura M, Imamura N, Kusaba H, Teraoka Y, Fuchino H, Tsujimoto K, Uchida Y, Jingo N (2006) J Electrochem Soc 153:A2023
3. Cheng Z, Zha SW, Aguilar L, Wang D, Winnick J, Liu ML (2006) Electrochem Solid State Lett 9:A31
4. Trembly JP, Marquez AI, Ohrn TR, Bayless DJ (2006) J Power Sour 158:263
5. Cheng Z, Zha SW, Liu ML (2007) J Power Sour 172:688
6. Mukundan R, Brosha EL, Garzon FH (2004) Electrochem Solid State Lett 7:A5
7. Yi YF, Rao AD, Brouwer J, Samuelsen GS (2005) J Power Sour 144:67
8. Trembly JP, Gemmen RS, Bayless DJ (2007) J Power Sour 163:986
9. Xu ZR, Luo JL, Chuang KT (2007) J Electrochem Soc 154:B523
10. Centi G, Cavani F, Trifiro F (2000) Selective oxidation by heterogeneous catalysis. Kluwer, New York
11. Karamullaoglu G, Dogu T (2007) Ind Eng Chem Res 46:7079
12. Ishaque Khan M, Deb S, Marshall CL (2009) Catal Lett 128:256
13. Daniell W, Ponchel A, Kuba S, Anderle F, Weingand T, Gregory DH, Knoezinger H (2002) Top Catal 20:65
14. Katagiri T, Nakamura Y Japan Patent 08187430 A2 19960723
15. Wang Y, Liu Z, Zhen Y, Zhan L, Huang Z, Liu Q, Ma QJ (2004) Chem Eng Sci 59:5283
16. Taguchi H, Matsuura SI, Nagao M, Kido H (1999) Phys B 270:325
17. Boroomand F, Wessel E, Bausinger H, Hippert K (2000) Solid State Ion 129:251
18. Saracco G, Scibilia G, Iannibello A, Baldi G (1996) Appl Catal B 8:229
19. Zwinkels MFM, Hanssner O, Menon PG, Jaras SG (1999) Catal Today 47:73
20. Peng C, Liu YN, Zheng YX (2003) Mater Chem Phys 82:509
21. Milby TH, Bselt RC (1999) Am J Ind Med 35:192
22. Rida K, Benabbas A, Bouremmad F, Pena MA, Sastre E, Martinez-Arias A (2007) Appl Catal A Gen 327:173
23. Nakano H, Kawakami S, Fujitani T, Nakamura J (2000) Sur Sci 454:295
24. Botte G, Muthuvel M, Marquez A, Office of Fossil Energy Fuel Cell Program. FY 2006 Annual Report P91